Residual Stress Evolution in Zirconia (Y8%) Coatings During Atmospheric Plasma Spraying for Substrates Under Rotating Kinematic

Vincent Lasseur, Simon Goutier, Venancio Martinez Garcia, Alain Denoirjean, Erick Meillot, Gilles Mariaux, Joseph Absi, Andreas Killinger

Residual Stress Evolution in Zirconia (Y8%) Coatings During Atmospheric Plasma Spraying for Substrates Under Rotating Kinematic

V. Lasseur[1] · S. Goutier[1] · V. Martinez Garcia[2] · A. Denoirjean[1] · E. Meillot[3] · G. Mariaux[1] · J. Absi[1] · A. Killinger[2]

Abstract Ceramics coatings produced by atmospheric plasma spraying (APS) on steel alloys parts involve high residual stress level that can affect the coating properties and integrity. Most of the experimental studies were focused on the stress evaluation into APS-produced coatings onto static targets. However, these studies have not been extended to stresses induced on rotating samples. Indeed, the thermal background and the deposition way onto a static target is different from a rotating one, resulting in indifferent coating residual stresses. The aim of this work is to estimate and understand the real-time stress evolution from the sandblasting process to the coating formation while the substrate is fixed at a rotating support thanks to a new system developed in the laboratory. Three different sources of stresses are analyzed in this paper: stresses induced by sandblasting, substrate heating, and splat quenching followed by the cooling down of the coating/substrate composite. Resulting stresses measurements are compared with after test ones made by incremental hole drilling.

Keywords atmospheric plasma spraying (APS) · residual stress · rotating kinematic · thermal barrier coating (TBC) · yttria-stabilized zirconia (YSZ)

[1] Univ. Limoges, CNRS, IRCER, UMR 7315, 87000 Limoges, France

[2] Univ. Stuttgart, IFKB, Allmandring 7b, 70569 Stuttgart, Germany

[3] CEA-DAM, Le Ripault, 37260 Monts, France

Introduction

Atmospheric plasma spraying (APS) is a widely used deposition process that allows to build ceramic or metallic thick coating by stacking of lamellas formed by crushing of molten and accelerated powder particles by a thermal plasma jet. These coatings are commonly used as thermal barriers, wear, oxidation or corrosion protection, surface reloading. (Those particles are propelled toward the substrate in order to build a deposit with adapted conditions depending on the final properties required.)

Coatings lifetime is a research issue that has been proven to be affected by residual stresses (Ref 1). Sprayed coatings show internal stresses related to the deposition process history that can affect the coating integrity if the process is not well controlled (i.e., delamination effects) especially for thermal applications (Ref 2). Those stresses are an addition of processing steps: grit blasting, particles quenching during coating buildup, and thermal cooling after spraying.

Grit blasting residual stresses are induced by the multiple impact of hard sharp ceramic elements onto the specimen surface. It leads to a specific surface increase and induces a material compression stress state extending beneath the surface (Ref 3).

Quenching stresses results from rapid solidification of melted particles during deposit buildup. As the thermal transfer of each particles is 10^6 to 10^8 K s^{-1} and the delay

between two particles impact is around 100 μs (Ref 4), no interactions between particles is achieved and a first approximation of quenching stress can be calculated as follows (Ref 5):

$$\sigma_{Q_0} = \alpha_c \cdot \frac{E_c}{1 - \nu_c} \cdot (T_m - T_s)$$

where E_c is the coating Young's modulus, ν_c is the coating Poisson ratio, α_c is the coefficient of thermal expansion of the coating, T_m is the melting temperature of the coating material, and T_s is the substrate temperature during deposition. Compared to experimental results, higher stress values are obtained from such calculation. This difference is due to crack formation into splats after cooling which release internal stresses (Ref 5).

Thermal stresses emerge during cooling from deposition temperature to ambient one due to the thermal expansion coefficient misfit between the substrate and deposited material. This stress can be calculated as:

$$\sigma_{Th_d} = \frac{E_c}{1 - \nu_c} \cdot (\alpha_s - \alpha_c) \cdot (T_s - T_{amb})$$

where α_s is the substrate coefficient of thermal expansion, T_s the substrate temperature during deposition and T_{amb} the room temperature. Such calculation is accurate as long as no cracks appear (Ref 6).

In situ curvature measurement of substrates during APS process is a powerful tool to quantify stresses formation (Ref 7). Curvature data capture allows to study stresses origins during the process. Such device is used on fixed plane conventional parts (ICP—in situ coating property) and has not yet been expanded to rotary substrates. Based on the curvature study, another device should be mentioned: DIC (digital image correlation) (Ref 8), such device allows high accuracy up to phase transformation occurring in YSZ and multilayered materials study. As this study is focused on stabilized YSZ (8%) and bimaterials, ICP device model will be preferred for this study.

Mutter et al. study (Ref 9) highlighted stresses relaxation effects from first layers deposition and after deposition without being able to split the different phenomena occurring for a fixed plane part. This study aims to clarify each phenomena role by using rotating substrates. Such pattern induces slower layering buildup allowing better vision on each phenomenon. A comparison between both patterns is also presented.

Experimental Methods

Substrate Preparation and Spraying Conditions

In this study, A-type Almen strip is used as substrate. Grit blasting surface preparation has been proceeded using alumina grit (ϕ = 1 mm), and an air pressure of 2 bar resulting in a surface roughness of R_a = 3.9 ± 0.5 μm. Commercial powder 8 wt.% YSZ powder Metco 204AF with size distribution − 45 + 15 μm was used as coating material. Sample and coating material bulk elastic properties are shown in Table 1. The powder was plasma-sprayed under atmospheric conditions (APS) using an Oerlikon Metco F4 plasma torch with a 6-mm exit nozzle. Spraying conditions are documented in Table 2; gun current is kept constant at 500 A, voltage around 65 V and cooling power at 15 kW. Spray distance is 100 mm. Before coating deposition, twenty preheating passes are performed in order to achieve sample temperature and curvature equilibrium. An Ar/H_2 mixture is used (33/10 slpm).

Spraying Pattern

Two plasma jet patterns are compared (Fig. 1):

- A planar one corresponding to horizontal and vertical torch movements in front of a fixed substrate. A 4 mm step is applied, and a 200 mm/s torch translation speed is a fixed;
- A rotating one corresponding to vertical torch movements in front of a rotating substrate. An identical 4 mm step is obtained (substrate speed: 200 rpm, torch travel speed: 13.3 mm/s).

In Situ Curvature Measurement

Experimental setup is shown in Fig. 2. Sample curvature was recorded during deposition process and post-deposition cooling using a device developed in the laboratory for samples in rotating kinematic. A 180-mm-diameter cooled double walled cylinder is used as both sample holder and shield for electronic measurement equipment. Wireless transmission data are achieved between sensors and data acquisition system.

Specimens are fixed using a clamping system on one side allowing the "beam" to bend freely. A non-contact laser displacement sensor with 30 μm resolution is used to measure its deflection at the opposite side. As only one sensor is used, system body displacement has been checked

Table 1 Materials parameters used for calculation

	SAE 1070	YSZ
E Young's modulus, GPa	209	100
v Poisson ratio	0.29	0.22

Data for SEA 1070 are taken from SubsTech database and YSZ from manufacturer (Oerlikon-Metco)

with non-sandblasted samples and no thermal or kinematic mode effect was detected. Sample curvature κ was calculated from displacement at 60 mm from clamping area as:

$$\kappa = \frac{2f}{(l^2 + f^2)}$$

where l is the sample length and f is the measured displacement.

Table 2 Spraying conditions applied

Feed rate, g min^{-1}	Thickness, μm	Dep. passes
20	100	35
20	200	35
20	400	35
60	200	11

A typical curvature change versus time is shown in Fig. 3. Such evolution can be decomposed in three phases:

- A preheating phase which involves an increase in curvature;
- A deposition phase which can be divided into two phases:
  - A steep initial increase in curvature due to stress releasing;
  - A linear evolution due to coating buildup;
- A cooling phase involving the thermal coefficients mismatch (between YSZ and SAE 1070) leading to compressive stress formation (Ref 10).

The sample temperature was measured with a RAYMID 20-LT CB3 monochromatic optical pyrometer focused on the middle of the specimen front side. The device has a 150 ms response time and a wavelength between 8 and 14 μm. Deposition temperature is defined as the average

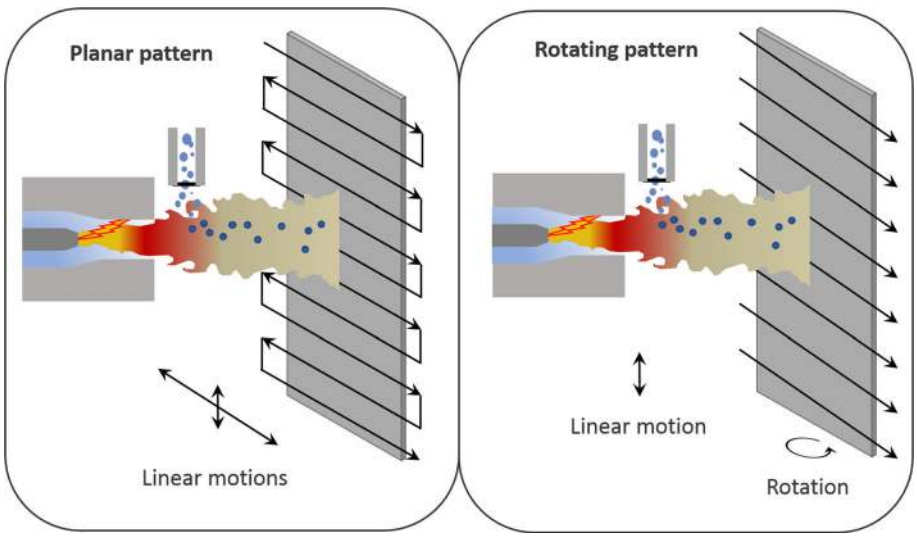

Fig. 1 Torch pattern onto substrate surface

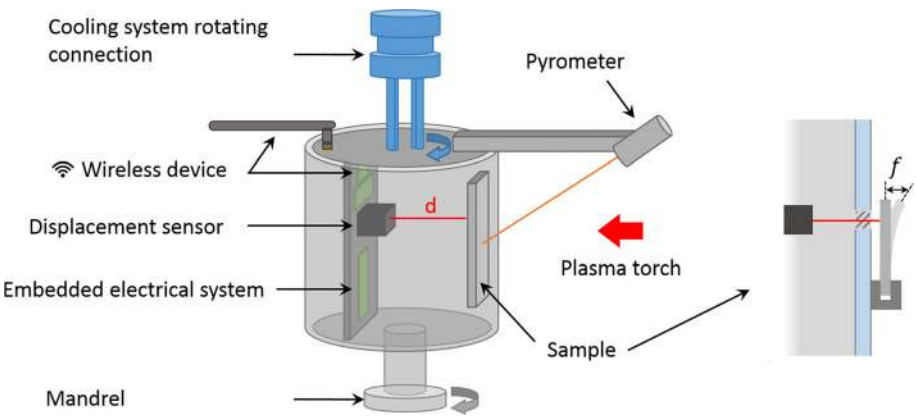

Fig. 2 In situ curvature measurement device for rotary applications

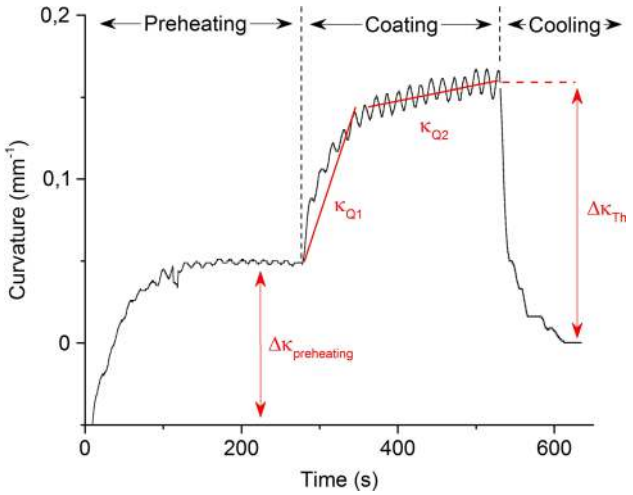

Fig. 3 Typical example of curvature increase for YSZ on Almen strip

temperature during the coating building.

Coating Stress Calculation

Following Brenner and Senderoff calculation (Ref 11), quenching and thermal stresses can be determined measuring the curvature change during APS. This calculation, based on Stoney's equation (Ref 12), which is derived from bending moments, forces balances and the assumption of pure elastic deformations. It allows studying thicker coatings up to a coating/substrate ratio of 0.5. As the curvature first steep increase is identified as heating phenomenon, it has not been considered in calculations and thus only particles quenching is accounted:

$$\sigma_{Q} = \frac{E_c}{6 \cdot (1 - \nu_c)} \cdot \frac{t_s\left(t_s - \beta^{5/4} t_c\right)}{t_c} \cdot \Delta\kappa_{Q}$$

$$\beta = \frac{E_c}{E_s} \cdot \frac{(1 - \nu_s)}{(1 - \nu_c)}$$

where σ_Q is the average quenching stress in the coating, E is the Young's modulus, ν the Poisson ratio, t the thickness and subscripts s and c refer to substrate and coating.

Thermal stress calculation σ_{Th} can be determined using the following equation (Ref 5):

$$\sigma_{Th_d} = \frac{E_c}{1 - \nu_c} \cdot (\alpha_s - \alpha_c) \cdot (T_s - T_{amb})$$

The bulk materials elastic properties used for calculations are summarized in Table 1.

At least two samples were studied for each condition.

Residual Stress In-Depth Profile Measurement

An incremental orbital hole drilling method (Ref 13) has been used to quantify in-depth residual stresses of specimens at room temperature. The method is well adapted to plasma coatings regarding deposit depth and the possibility to consider bimaterials systems.

The process creates a cylindrically shaped hole with a 1 mm diameter with a 0.7-mm diamond drill. The hole is drilled by 10-µm step. High-speed drilling (300,000 rpm) and low penetration rate (around 60 µm min^{-1}) are performed and guarantee a stress-free drilling process with negligible heat development. Four strain gauges are bonded on the substrate surface radially around the drilling region using methacrylate and benzoyl peroxide mixture.

Thus, for every incremental steps of hole drilling, the residual stresses in the specimen are locally released due to the material removal, leading to a deformation of the surface around the hole measured by the strain gauges. Thanks to elastic material properties (i.e., Young's modulus and Poisson ratio), it is possible to calculate in-depth residual stresses.

Results and Discussion

As surface roughness enhance considerably the mechanical bonding between coating and substrate, samples were prepared by grit blasting. This process enlarges the specific substrate surface but also induces compressive residual stress in the substrate due to elasto-plastic deformation corresponding to local hardening (Ref 13).

Specimen Preheating Curvature Increase

Figure 4 shows the evolution of preheating curvature versus time of a grit-blasted A-type Almen strip. The curvature noise is attributed to the plasma plume movements over the sample inducing an effect of plasma momentum on the specimen. One can see a steep increase in curvature during the first seconds followed by an asymptotic tendency. The value of the asymptotic trend depends on temperature.

This evolution is largely affected by the grit blasting process as the curvature of non-grit-blasted substrate remains rather constant with temperature contrary to a grit-blasted one. Figure 5 shows the curvature change during preheating followed by cooling of a grit-blasted Almen strip. A quasi absence of curvature at the end (t = 300 s) contrary to the beginning (t = 0 s) indicates an internal change of residual stress. The residual stress in-depth profile measured by hole drilling up to 0.5 mm (substrate is 1.3 mm thick) shown in Fig. 6 highlights this change. As

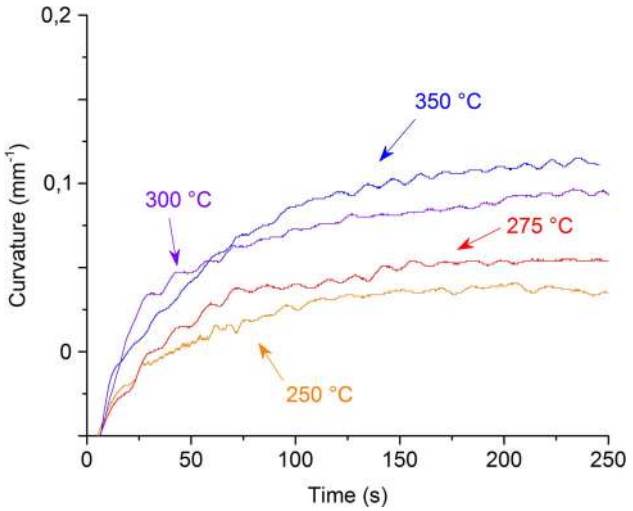

Fig. 4 Curvature development during preheating by plasma plume of a one-side sandblasted (F20, 2 bar) Almen strip (SAE 1070 iron) for four temperatures

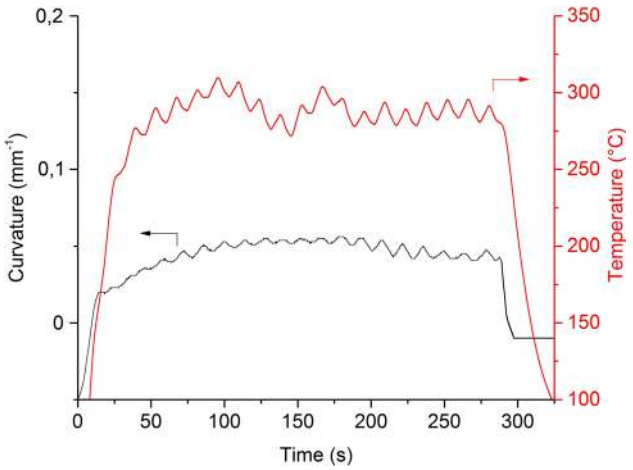

Fig. 5 Curvature development during preheating by plasma plume of a one-side sandblasted (F20, 2 bar) Almen strip (SAE 1070 iron)

expected, a compressive state is found in the substrate after grit blasting. The surface compressive residual stress decreases from approximately − 400 to − 100 MPa after heating. A maximum residual stress beneath the surface at 50 µm of − 250 MPa is kept following preheating of the grit-blasted specimens.

Coating Formation

The samples curvature has been recorded during deposition and cooling in order to calculate residual stresses within the coating. During the deposition step, a steep increase in curvature during the first deposited layers is observed for various spray conditions (Ref 9). An example of such increase is shown in Fig. 3 (area 1).

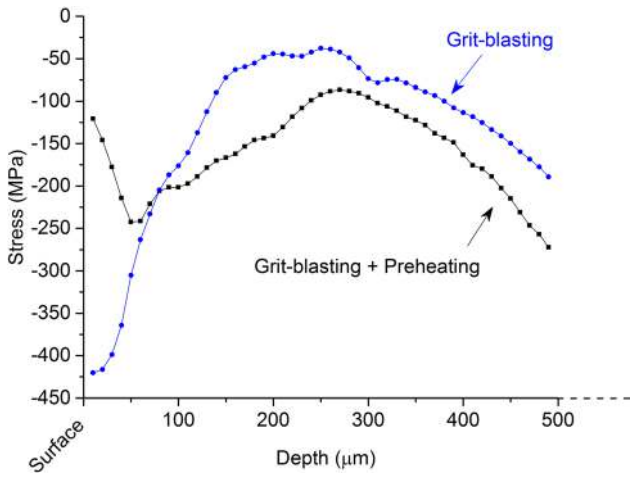

Fig. 6 In-depth residual stress profile by incremental hole drilling for SAE 1070 substrate grit blasted (F20, 2 bar) and, with and without preheating (300°C)

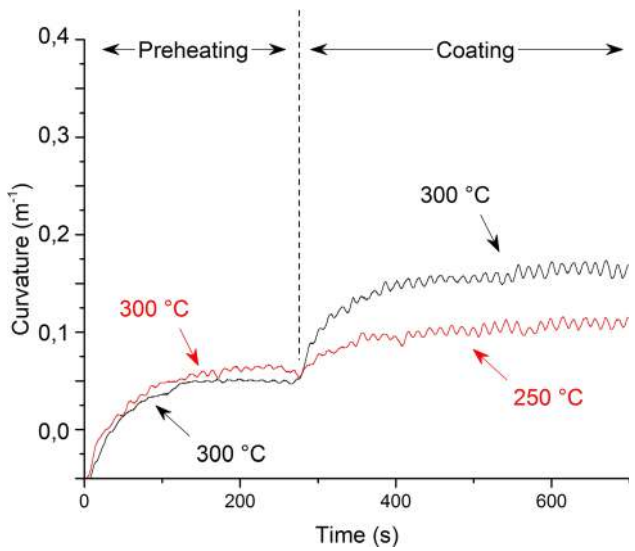

Fig. 7 Curvature development during preheating of a one-side sandblasted (F20, 2 bar) Almen strip (SAE 1070 iron) at 300°C followed by YSZ first layers deposition at 250 and 300°C

Initial Curvature Increase

The initial curvature steep increase is explained by two possible reasons in literature:

- A thermal transfer between particles and substrate during particles cooling on the substrate surface due to local temperature increase (Ref 14).
- The creation of an interface layer with better bonding due to surface roughness involving higher stress formation (Ref 9).

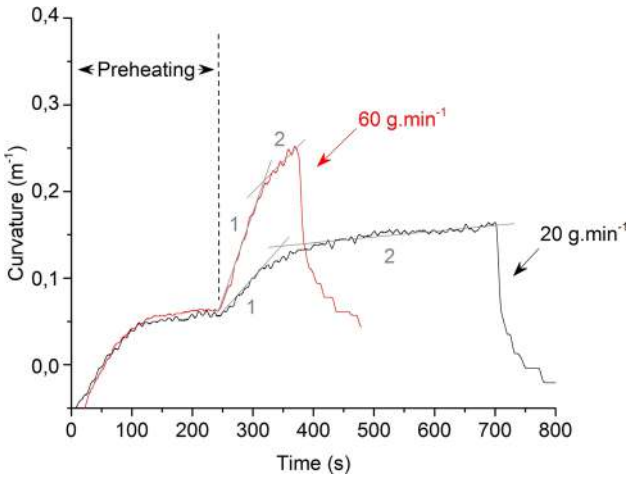

Fig. 8 Curvature development during preheating of a one-side sandblasted (F20, 2 bar) Almen strip (SAE 1070 iron) at 300°C followed by YSZ deposition at 300°C for two powder feed rates (20 and 60 g min^{-1})

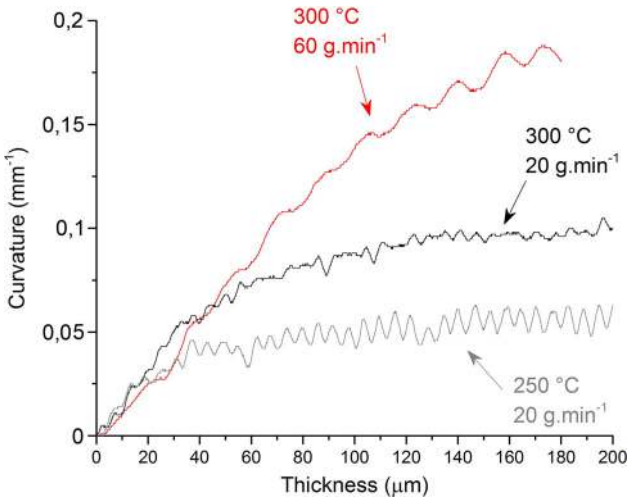

Fig. 9 Curvature development during deposition of YSZ on a one-side sandblasted (F20, 2 bar) Almen strip (SAE 1070 iron) at 300°C for two powder feed rates (20 and 60 g min^{-1})

Figure 7 shows the steep increase in curvature during an YSZ coating buildup on an Almen strip (SEA 1070 steel) for two deposition temperatures. The temperatures were obtained by adjusting the cooling air flow. The same preheating temperature has been applied and the deposition passes rate has been kept similar for both conditions. A strong dependency between curvature increase and deposition temperature can be observed during the deposition of the first layers. However, for a condition with identical preheating and deposition temperatures, a curvature increase is still obtained for the first layers created.

In order to discuss the interface creation and its link to the steep increase, Fig. 8 shows the specimen curvature development for two powder feed rates. Increasing the feed rate leads to thicker layers, a steeper curvature change and thus higher stresses. Thus, a powder feed rate increase implies more particles per second impacting on the substrate, and therefore, a thermal transfer increase should result in a steeper curvature. As one can see in Fig. 8, a faster curvature increase is observed for a feed rate of 60 g min^{-1}.

However, as Fig. 9 shows, curvature change versus deposition thickness is identical for the first 20 µm deposited no matter powder feed rate or deposition temperature (layers thickness is assumed identical along coating creation).

As a conclusion, the curvature steep increase can be linked mostly to the particles heat transfer. For an identical preheated substrate, until 20 µm deposited an identical curvature is observed, but lower operating temperature induces less curvature after this threshold. Layers thickness, on another hand, does not show any impact before 40 µm.

Stresses Calculations

As the steep increase in area 1 has been identified as stress release by heat transfer, not only quenching stresses are involved. Thus, stresses calculations from curvature are performed only with area 2 (Fig. 8).

Residual stresses calculated from Fig. 8 conditions are presented in Table 3. As expected, higher residual stresses are obtained for thicker layers built-up deposit.

Two deposition thicknesses have been studied: 100 and 400 µm. Figure 10 shows the curvature development for preheating and spraying at 300°C. A steady curvature development is observed for the 400 µm coatings leading to a steady increase in quenching stresses along coating creation. As expected, higher tensile stresses are found on thicker samples up to 70 MPa. The thermal compressive stresses behavior is identical considering that every deposit has been created at same temperature. A circular pattern for deposition induces low quenching stresses compared to planar setup (Ref 10), and therefore, an overall compressive residual stress is achieved for every sample.

Those calculations aim to evaluate stress formation during plasma spraying. Considering that, as shown in Fig. 6, specimens state before coating is not stress free and in order to evaluate the impact of the grit blasting stresses on the specimen residual stress, incremental hole drilling has been performed. Results are shown in Fig. 11 for a 0.5 mm depth; one can see an increase in the interface compressive stress as the deposit depth increases. Stress calculation from curvature is accurate for 100 µm deposit with a mean calculated value of 50 MPa. Formation of a thicker coating leads to an internal relocation of the

Table 3 Stresses calculation by curvature measurement for coating depths of 100 and 400 µm (300°C preheating and deposition)

Feed rate, g min^{-1}	Thickness, µm	σ_Q, MPa	σ_{Th}, MPa	σ_R, MPa
20	100	17	− 71	− 54
20	200	37	− 71	− 37
20	400	70	− 71	− 1
60	200	53	− 71	− 18

Data errors are estimated as ± 2 MPa for σ_Q, ± 4 MPa for σ_{Th} and ± 6 MPa for σ_R

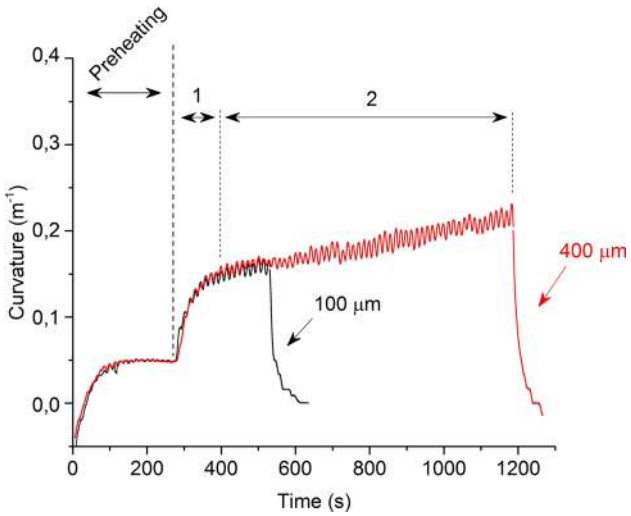

Fig. 10 Curvature development during preheating of a one-side sandblasted (F20, 2 bar) Almen strip (SAE 1070 iron) at 300°C followed by YSZ deposition at 300°C for two deposit depth: 100 and 400 µm

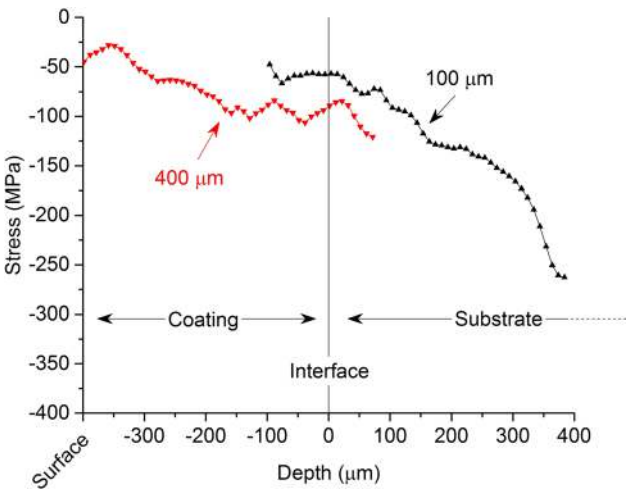

Fig. 11 In-depth residual stress profile by incremental hole drilling for SAE 1070 substrate grit blasted (F20, 2 bar), preheated at 300°C and YSZ coated at 300°C. Two conditions are studied: deposit depth of 100 and 400 µm

maximum compressive stress from grit blasting and, as a result, the interface stress gets wider and calculation shows differences from incremental hole results.

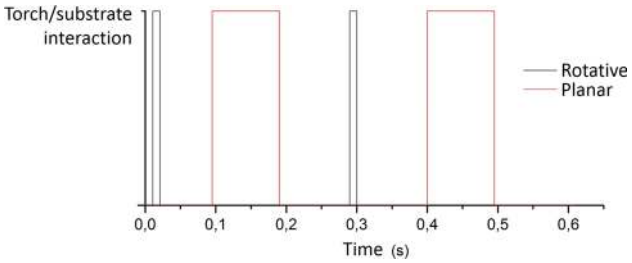

Fig. 12 In time torch/substrate interaction example during 0.6 s

Pattern Study

Two hundred-µm-thick coatings are produced with identical deposition rate of 65 µm/s following two different plasma torch patterns, rotating and planar. Figure 12 highlights that the torch/substrate interaction time during spraying is shorter for a rotative pattern than for a plane one.

Microstructures

Coating SEM cross sections observation (Fig. 13) shows interlamellar cracks for the planar pattern. Such phenomenon is due to coating stresses accumulation exceeding the material resistance and leading to a crack releasing state (Ref 15). Rotative pattern is crack-free.

Curvature Comparison

Preheating curvature change is almost identical (Fig. 14). Considering the pattern differences, achieving an identical preheating temperature is almost impossible. A higher preheating temperature was chosen in order to highlight the coating first layer's influence onto curvature change.

As the coating is created, an initial curvature decrease is achieved for rotating pattern. As shown before, first layers curvature change is strongly linked to deposition temperature for this setting. On the contrary, a planar pattern shows no curvature differences between firsts and following layers created. Such pattern involves higher stresses input during coatings creation.

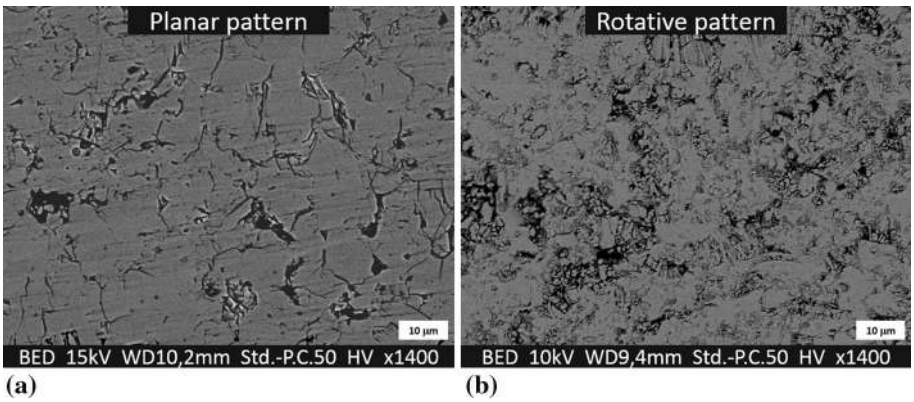

Fig. 13 SEM cross sections of Zirconia (8%) coatings for (a) planar and (b) rotative patterns

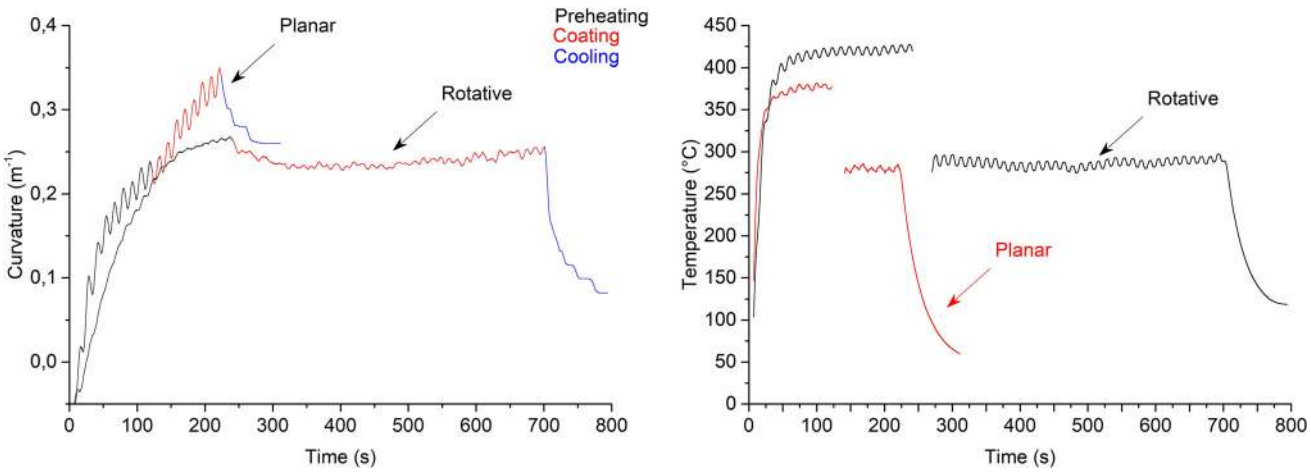

Fig. 14 Curvature development during preheating of a one-side sandblasted (F20, 2 bar) Almen strip (SAE 1070 iron) at 400°C followed by YSZ deposition at 300°C for two patterns (rotative and planar)

Table 4 Stresses calculation by curvature measurement for 200 µm coatings (400°C preheating/300°C deposition)

Pattern	σ_Q, MPa	σ_{Th}, MPa	σ_R, MPa
Planar	51	− 83	− 32
Rotative	10	− 83	− 73

Data errors are estimated as ± 2 MPa for σ_Q, ± 4 MPa for σ_{Th} and ± 6 MPa for σ_R

Stress Study

Curvature-related stress calculations are presented in Table 4. A good accuracy is obtained for both patterns. Higher residual stresses are obtained for planar pattern. In substrate depth, stresses are present due to longer deposition time, and thus, more thermal stress release effects. These calculations agree with incremental hole drilling results (Fig. 15).

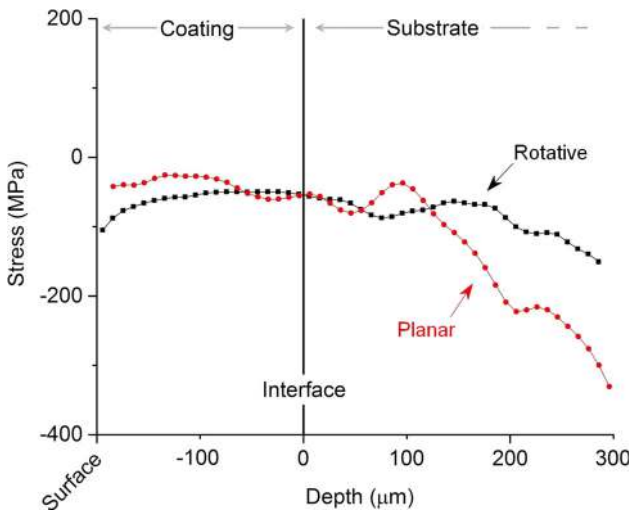

Fig. 15 In-depth residual stress profile by incremental hole drilling for SAE 1070 substrate grit blasted (F20, 2 bar), preheated at 400°C and YSZ coated at 300°C. Two patterns are studied: rotative and planar 200-µm-thick coatings

Summary and Conclusion

Investigations with a rotating deposition pattern by APS of YSZ onto Almen strip showed the critical impact of operating temperatures. The preheating thermal treatment decreases the surface residual stresses induced by grit blasting allowing substrate to reach curvature equilibrium. However, an in-depth study of residual stress reveals remaining stresses under the surface which are also visible after deposition process. Such observation highlights the grit blasting conditions prominence on the final residual stress state of specimens.

Curvature studies during the first deposition layers revealed stress releasing due to particles heat transfer during their cooling on the substrate surface. A curvature steep increase results from this phenomenon and is gradually overwhelmed by the particles quenching stresses when a new thermal equilibrium is reached.

The results strongly indicate the sliding of maximum compressive stresses induced by grit blasting as the deposit depth increases. Such tendency would lead to critical stresses at interface which can be responsible for delamination effects. Therefore, stresses calculation from curvature is more accurate for thinner deposit (i.e., as long as substrate's residual stresses do not get involved).

Finally, higher stresses are generated for planar pattern in comparison to rotating one, leading to sandblasting on curvature change effect hided during coating creation.

References

1. R. Vaβen, S. Giesen, and D. Stöver, Lifetime of Plasma-Sprayed Thermal Barrier Coatings: Comparison of Numerical and Experimental Results, *J. Therm. Spray Technol.*, 2009, **18**(5-6), p 835
2. J.W. Watson and S.R. Levine, Deposition Stress Effects on the Life of Thermal Barrier Coatings on Burner Rigs, *Thin Solid Films*, 1984, **119**(2), p 185-193
3. M. Mellali, A. Grimaud, A. Leger, P. Fauchais, and J. Lu, Alumina Grit Blasting Parameters for Surface Preparation in the Plasma Spraying Operation, *J. Therm. Spray Technol.*, 1997, **6**(2), p 217
4. A. Vardelle, C. Moreau, and P. Fauchais, The Dynamics of Deposit Formation in Thermal-Spray Processes, *MRS Bull.*, 2000, **25**(7), p 32-37
5. S. Kuroda and T. Clyne, The Quenching Stress in Thermally Sprayed Coatings, *Thin Solid Films*, 1991, **200**(1), p 49-66
6. V. Teixeira, Mechanical Integrity in PVD Coatings due to the Presence of Residual Stresses, *Thin Solid Films*, 2001, **392**(2), p 276-281
7. J. Matejicek and S. Sampath, In Situ Measurement of Residual Stresses and Elastic Moduli in Thermal Sprayed Coatings: Part 1: Processing Effects on Properties of Mo Coatings, *Acta Mater.*, 2003, **51**(3), p 863-872
8. B.P. Croom, C. Bumgardner, and X. Li, Unveiling Residual Stresses in Air Plasma Spray Coatings by Digital Image Correlation, *Extrem. Mech. Lett.*, 2016, **7**, p 126-135
9. M. Mutter, G. Mauer, R. Mücke, R. Vaβen, H.C. Back, and J. Gibmeier, Investigations on the Initial Stress Evolution During Atmospheric Plasma Spraying of YSZ by In Situ Curvature Measurement, *J. Therm. Spray Technol.*, 2016, **25**(4), p 672-683
10. M. Mutter, G. Mauer, R. Mücke, O. Guillon, and R. Vaβen, Correlation of Splat Morphologies with Porosity and Residual Stress in Plasma-Sprayed YSZ Coatings, *Surf. Coat. Technol.*, 2017, **318**, p 157-169
11. J. Matejicek, S. Sampath, D. Gilmore, and R. Neiser, In Situ Measurement of Residual Stresses and Elastic Moduli in Thermal Sprayed Coatings: Part 2: Processing Effects on Properties of Mo Coatings, *Acta Mater.*, 2003, **51**(3), p 873-885
12. G.G. Stoney, The Tension of Metallic Films Deposited by Electrolysis, *Proc. R. Soc. Lond. Ser. A, Contain. Pap. Math. Phys. Character*, 1909, **82**(553), p 172-175
13. R. Gadow, M. Riegert-Escribano, and M. Buchmann, Residual Stress Analysis in Thermally Sprayed Layer Composites, Using the Hole Milling and Drilling Method, *J. Therm. Spray Technol.*, 2005, **14**(1), p 100-108
14. M. Mellali, Influence de la rugosité et de la température de surface du substrat sur l'adhérence et les contraintes résiduelles au sein de dépôts d'alumine projetés par plasma (Substrate roughness and surface temperature impact on plasma sprayed alumina adhesion and residual stresses), Ph.D. Thesis, (Limoges University, 1994) (**in French**)
15. B.D. Choules, K. Kokini, and T.A. Taylor, Thermal Fracture of Ceramic Thermal Barrier Coatings Under High Heat Flux with Time-Dependent Behavior: Part 1 Experimental Results, *Mater. Sci. Eng., A*, 2001, **299**(1-2), p 296-304